19th International Conference on the Computation of Electromagnetic Fields

Technical Program

Compumag 2013

30 June–4 July 2013, Budapest, Hungary

	PD6-14 **Numerical and Experimental Design Validation for Optimal Efficiency Distribution Compatible to Frequent Operating Range of Interior PMSM** Hochang Jung[1], Jihyun Ahn[2], Deokjin Kim[1], Sang-Yong Jung[2] [1]Korea Automotive Technology Institute(KATECH), Republic of Korea (South Korea); [2]Sungkyunkwan University, Republic of Korea (South Korea) **PD6-15** **Design of a BLDC Motor for Low Cost and Low Noise Application** Sangkla Kreuawan[1], Nattapon Chayopitak[1], Prasit Champa[1], Pakasit Somsiri[1], Sisuda Chaithongsuk[2] [1]National Electronics and Computer Technology Center; [2]Rajamangala University of Technology Suvarnabhumi **PD6-16** **Design of a Vernier Machine with Permanent Magnet on both sides of Rotor and Stator** Ho min Shin, Dae Kyu Jang, Jung Hwan Chang Dong-A University, Republic of Korea (South Korea) **PD6-17** **Influences of Isotropic and Anisotropic Magnetostriction on Three-Phase Transformer with Highly Grain-Oriented Electrical Steel Sheet** Heesung Yoon, C.S. Koh Chungbuk National University, Republic of Korea (South Korea) **PD6-18** **Finite-Element Analysis of Demagnetization of IPM-type BLDC Motor with Stator Turn Fault** Yoon-Seok Lee, Jin Hur University of Ulsan, Republic of Korea (South Korea) **PD6-19** **A study on IPMSM Design for Sensorless Control with High-Frequency Voltage Signal Injection** Seung-Hee Chai[1], Myung-Seop Lim[1], Jae-Woo Jung[1], Jung-Pyo Hong[1], Seung-Ki Sul[2] [1]Hanyang University, Republic of Korea (South Korea); [2]Seoul National University, Republic of Korea (South Korea) **PD6-20** **Analytical Model of Induction Motor for Performance Calculation** Ankit Dalal, Mohammed Nasir Ansari, Praveen Kumar Indian Institute of Technology, Guwahati., India **PD6-21** **Analysis of Temperature Distribution on Power Switches Arrangements in Power Converter for Switched Reluctance Motor Drive** Hao Chen, Yang Xu China University of Mining & Technology, People's Republic of China
3:25pm - 3:50pm	**Coffee Break**

A study on IPMSM Design for Sensorless control with High-Frequency Voltage Signal Injection

Seung-Hee Chai[1], Myung-Seop Lim[1], Jae-Woo Jung[1], Jung-Pyo Hong[1], *Senior Member, IEEE* and Seung-Ki Sul[2], *Fellow member*, IEEE

[1]Department of Automotive Engineering, Hanyang University, Seoul 133-791, Korea
[2]School of Electrical and Computer Engineering, Seoul National University, Seoul 151-742, Korea

This paper presents the reasons for error resulting from the position estimation method of sensorless control, and presents the proper inductance distribution of the Interior Permanent Magnet Synchronous Motor (IPMSM) for sensor-less-oriented design based on high-frequency voltage signal injection. In order to find a solution to this problem, the cause of the estimating position error is established, and the concept of IPMSM for sensor-less oriented design is proposed. In this concept, as the Total Harmonic Distortion (THD) of the phase inductance in specific load conditions is decreased, the rotor position is better estimated. The inductance distribution based on the high-frequency voltage signal injection is compared with the test results. Both the simulation error patterns and the experiments are presented to verify the validity of the established method.

***Index Terms*—AC motor drives, IPMSM, sensorless control, phase inductance, total harmonic distortion.**

I. Introduction

TODAY, in an interior permanent magnet synchronous motor (IPMSM), there are several methods in sensor-less position control according to the operating speed. At low speed or standstill, the rotor position is estimated from the inductance distribution determined by the saliency of the magnetic path [1]. In an IPMSM, the permanent magnets (PM) have an effect on not only the induced back EMF, but the spatial saliency distribution. Non-uniformly positioned PM in the rotor cause the discrepancy between the *d-* and *q-axis* impedance which brings out the spatial saliency. With the high-frequency signal injection method, the position of the rotor can be estimated based on this saliency.

However, it is not easy to estimate the rotor position actually because the inductance profile is distorted by the means of core saturation with the input current under load conditions [2-5]. This distortion expresses the sum of many harmonic components, that is, the Total Harmonic Distortion (THD) of the phase inductance. Fortunately, the THD of the phase inductance can be reduced by a design change of the motor features.

In this paper, the reasons for error caused by the position estimation method are presented. In addition, how to design an electric motor for reducing the position error to the sensorless control is described.

II. Cause of the Inductance Computating Error in IPMSM for Sensorless control

A. Basic Principle of the High-frequency Rotating Voltage Signal Injection Method [1]

In sensorless control, the voltage equation of IPMSM in the stationary *d-/q-axis* reference frame with currents and flux can be described as (1)

$$\begin{bmatrix} v_{ds}^s \\ v_{qs}^s \end{bmatrix} = R_s \begin{bmatrix} i_{ds}^s \\ i_{qs}^s \end{bmatrix} + L_s \frac{d}{dt}\begin{bmatrix} i_{ds}^s \\ i_{qs}^s \end{bmatrix} + 2\Delta L\omega_r \begin{bmatrix} -\sin 2\theta_r & \cos 2\theta_r \\ \cos 2\theta_r & \sin 2\theta_r \end{bmatrix}\begin{bmatrix} i_{ds}^s \\ i_{qs}^s \end{bmatrix} + \omega_r \lambda_f \begin{bmatrix} -\sin\theta_r \\ \cos\theta_r \end{bmatrix} \quad (1)$$

where $[v^s_{ds}, v^s_{qs}]^T$ and $[i^s_{ds}, i^s_{qs}]^T$ are the vectors of the stator voltage, and the current in the stationary *d-/q-axis* reference frame, the inductance matrix, L_s, is represented in terms of the *d-/q-axis* inductances, and R_s, θ_r, λ_r and ω_r are the resistance, the rotor position, the permanent-magnet flux-linkage and the synchronous speed. Assume that the high-frequency voltage signal is injected into the IPMSM and the rotating speed is almost zero. In this case, the voltage drop of the resistance and the back EMF can be ignored. Then, the voltage equation of IPMSM in the rotor *d-/q-axis* reference frame is simply described as

$$\begin{bmatrix} v_{dsh}^r \\ v_{qsh}^r \end{bmatrix} = \begin{bmatrix} L_{ds} & 0 \\ 0 & Lqs \end{bmatrix}\frac{d}{dt}\begin{bmatrix} i_{dsh}^r \\ i_{qsh}^r \end{bmatrix} \quad (2)$$

According to the injected voltage signal, the current response can be derived from (2) as

$$\begin{bmatrix} i_{dsh}^r \\ i_{qsh}^r \end{bmatrix} = \int \begin{bmatrix} L_{ds} & 0 \\ 0 & L_{qs} \end{bmatrix}^{-1} \frac{d}{dt}\begin{bmatrix} v_{dsh}^r \\ v_{qsh}^r \end{bmatrix} dt \quad (3)$$

where $[v^r_{dsh}, v^r_{qsh}]^T$ and $[i^r_{dsh}, i^r_{qsh}]^T$ are the injected high-frequency voltage vector and the corresponding current vector in the synchronous rotor reference frame, respectively. The inductance matrix is represented in terms of the *d-/q-axis* inductance, L_{ds}, L_{qs}, in the synchronous rotor reference frame. From the current response, (2), the rotor position information can be extracted through a type of signal processing.

Manuscript received January 1, 2013. Corresponding author: Jung-Pyo Hong (e-mail: hongjp@hanyang.ac.kr).
Digital Object Identifier inserted by IEEE

B. *Cause of the estimating position error for sensorless control IPMSM*

In some IPMSMs, such as machines with high power density and speed range, variation of the inductance according to the rotor position is not sinusoidal because of the flux saturation caused by the input current under the load condition. Fig. 1 illustrates the pattern of the phase inductances and THD according to the change in the rotor position under no-load and load conditions. This shows that the harmonics appear in the inductance due to the flux saturation. If the phase inductance has *n-th* harmonic inductance, the harmonic inductance matrix, L_{abch} is expressed as

$$L_{abch} = L_h \begin{bmatrix} \cos 2\theta_r n & \cos 2n\left(\theta_r - \frac{\pi}{3}\right) & \cos 2n\left(\theta_r + \frac{\pi}{3}\right) \\ \cos 2n\left(\theta_r - \frac{\pi}{3}\right) & \cos 2n\left(\theta_r + \frac{\pi}{3}\right) & \cos 2\theta_r n \\ \cos 2n\left(\theta_r + \frac{\pi}{3}\right) & \cos 2\theta_r n & \cos 2n\left(\theta_r - \frac{\pi}{3}\right) \end{bmatrix} \tag{4}$$

where L_h is the amplitude of the harmonic inductance, and θ_r is the rotor position. Then, a 3-phase inductance matrix can be transformed to the *d-*, *q-axis* space harmonic profiles depending on the voltage injection angle as follows

$$[L_{sh}] = 1.5[T_{\theta r}][T_{dq}][L_{abch}][T_{dq}]^T[T_{\theta r}]^T \tag{5}$$

where, $[L_{sh}]$ and $[L_{abch}]$ are the inductance matrix of the *d-q* axis and the abc axis, $[T_{dq}]$ and $[T_{\theta r}]$ are the transformation matrix of the *d-q* transform and the rotational transform. The harmonic inductance matrix, L_{sh}, is represented in the synchronous rotor reference frame as

$$L_{sh} = \frac{3}{2}L_{mh}\begin{bmatrix} \cos 6\theta_r m & -\sin 6\theta_r m \\ -\sin 6\theta_r m & -\cos 6\theta_r m \end{bmatrix} \quad @\, n = 3m-1$$
$$L_{sh} = \frac{3}{2}L_{mh}\begin{bmatrix} \cos 6\theta_r m & \sin 6\theta_r m \\ \sin 6\theta_r m & -\cos 6\theta_r m \end{bmatrix} \quad @\, n = 3m+1 \tag{6}$$

where L_{mh} is the amplitude of the *n-th* harmonic inductance. The harmonic orders of the inductance are shown in Table I. The *6n-th* harmonics of the inductance, L_{sh}, in the synchronous rotor reference frame is calculated by any *n-th* phase harmonic inductance according to the rotor position. If the phase inductance has the *n-th* space harmonic inductance, the corresponding current response can be deduced as

TABLE I
HARMONIC ORDER OF L_{abch} AND L_{sh}

n	2	4	5	7	8	10	11	13	14	…
m	1	1	2	2	3	3	4	4	5	…
L_{SH}	6	6	12	12	18	18	24	24	30	6*n-th*

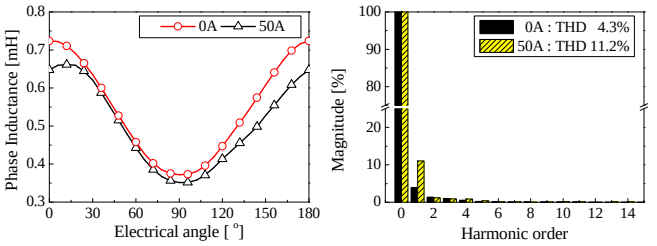

Fig. 1. Phase inductance profile as the rotor position changes under no-load and load conditions.

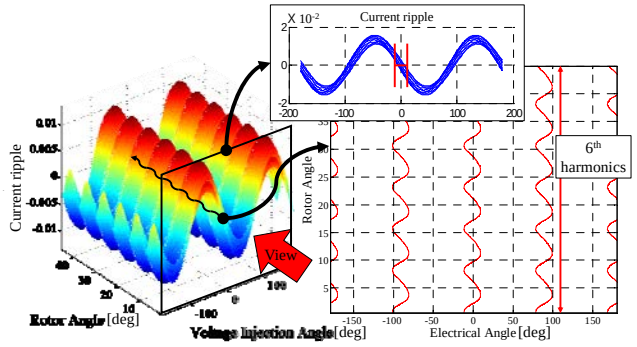

Fig. 2. Variation of the current ripple according to the rotor position (mechanical angle) and Voltage injection angle.

$$\begin{bmatrix} i^s_{dsh} \\ i^s_{qsh} \end{bmatrix} = \gamma \begin{bmatrix} \frac{\alpha}{\gamma}\cos\theta_r + \frac{\beta}{\gamma}\sin\theta_r \\ \frac{\alpha}{\gamma}\sin\theta_r - \frac{\beta}{\gamma}\cos\theta_r \end{bmatrix} \sin\omega_h t$$
$$= \gamma \begin{bmatrix} \cos(\theta_r - \rho) \\ \sin(\theta_r - \rho) \end{bmatrix} \sin\omega_h t \qquad \rho = \tan^{-1}\frac{\beta}{\alpha} \tag{7}$$

$$\alpha = A\frac{V_{inj}}{\omega_h}\left(L_{qsf} + L_{qsh}\right) \qquad \beta = A\frac{V_{inj}}{\omega_h}L^r_{qdsh}$$
$$A = \frac{1}{\left(L_{dsf} + L_{dsh}\right)\left(L_{qsf} + L_{qsh}\right) - L^r_{dqsh}L^r_{qdsh}} \tag{8}$$
$$\gamma = \sqrt{\alpha^2 + \beta^2}$$

where V_{inj} is the amplitude of the signal injection voltage, L_{sdf}, L_{qsf} are the *d-/q-axis* inductance of the fundamental, and L_{dsh}, L_{qsh} are the *d-/q-axis* inductance of the harmonic. The estimating rotor position errors, ρ, estimate the *6-th* harmonic, and they can be determined by

$$\rho = \tan^{-1}\frac{\beta}{\alpha} \approx \tan^{-1}\frac{-L_{mh}\sin 6\theta_r m}{L^r_{qsf}} \quad @\, n = 3m-1$$
$$\rho = \tan^{-1}\frac{\beta}{\alpha} \approx \tan^{-1}\frac{L_{mh}\sin 6\theta_r m}{L^r_{qsf}} \quad @\, n = 3m+1 \tag{9}$$

This error is displayed in the form of *6n-th* order harmonics, as shown in Fig. 2. However, there are ways to reduce the distortion of the phase inductance phase of the motor design, and this is discussed in the next section.

III. Concept of IPMSM for Sensorless-Oriented Design

A. Main motor parameter for sensorless control in IPMSM

The rotor position can be estimated more easily if the phase inductance distribution is sinusoidal. There are several methods in the design of IPMSM for reducing the THD of the phase inductance.

1. Electric loading/ magnetic loading
2. Winding conbinations

B. Electric-/magnetic-loading for sensorless control

In a hybrid electric vehicle traction motor, the motors use more flux weakening current in armature windings. However, the motor for sensorless control, the flux made by the PM must be greater than that made by the armature reation, since the rotor position is estimated by the fact that the low permeability of the PM which is located on *d-axis*. This means that the way to design IPMSM for sensorless control is to increase the magnetic loading while reducing the electric loading. In (10) and (11), the magnitude of the magnetic load and the electric load are described. B, L_{stk}, N_{ph} and D_r are the flux density, stack length, number of turn phase and rotor diameter, respectively, while p and m are the pole-pair number and the number of phases.

$$\phi = B \times \frac{\pi D_r L_{stk}}{2p} \quad [Wb] \tag{10}$$

$$A = \frac{2mN_{ph}I}{\pi D_r} \quad [A/m] \tag{11}$$

C. Windings combination of motor for sensorless control

The motor for sensorless control requires sinusoidal phase inductance distribution and a minimum flux distortion by armature reaction at the air gap. This means that the machine has to be designed to distribute the armature reaction as evenly as possible to take advantage of the sensorless drive. The Distortion of the phase inductance is reduced from the distributed winding type: the spatial core saturation is relieved by the structural magnetic path of the distributed winding type compared with those of the concentrated winding type.

Self- and mutual-inductances (L_a and M_a) are generally expressed in terms of permeance and the magneto-motive force shown in (12), (13) and (14). Both values can be derived by the magnetic energy and flux linkage as shown in [6]. In distributed windings, harmonic terms in the magneto-motive force (MMF) are contain fewer than those of the concentrated windings, as shown in Fig. 3.

$$L_a = \frac{1}{4}\int_0^{2\pi} \Lambda_{\theta_r} F_a{}^2 d\theta_r \tag{12}$$

$$M_a = \frac{1}{4}\int_0^{2\pi} \Lambda_{\theta_r} F_a F_b d\theta_r \tag{13}$$

$$F_a = \sum_{n=1}^{\infty} \frac{4Ni}{n\pi} \cos\left(\frac{n\pi}{12}\right) \cos(n\theta_r) \tag{14}$$

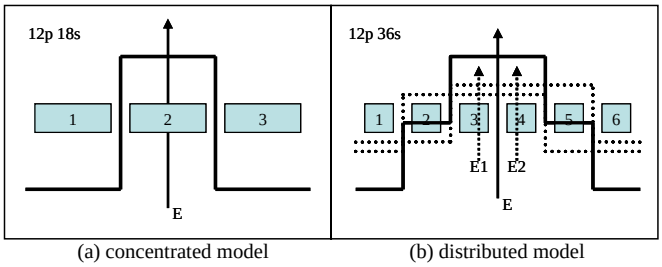

(a) concentrated model (b) distributed model

Fig. 3. MMF distribution of each models

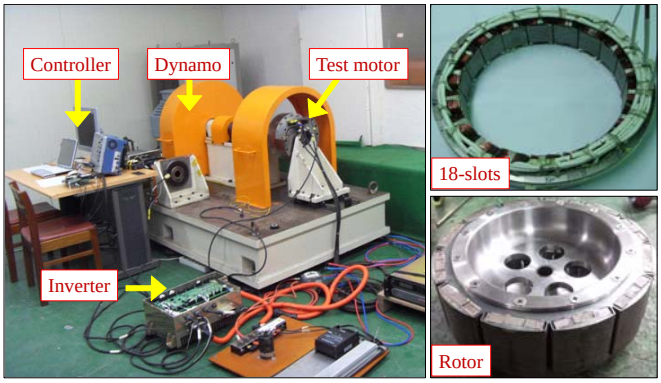

Fig. 4. Photographs of the test set

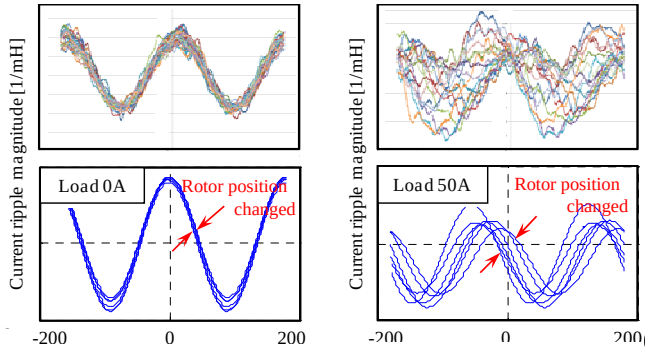

(a) No-load condition (b) 50A load condition

Fig. 5. Estimated current ripple(lower) and experimental result(upper)

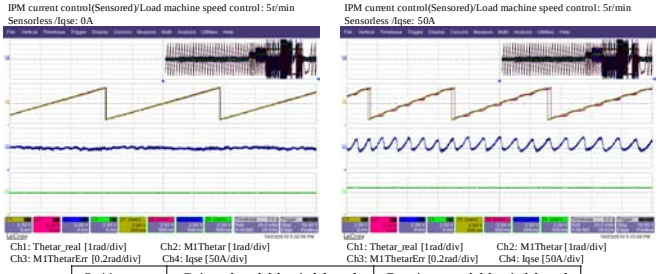

Position error	Estimated result [electrical degree]	Experiment result [electrical degree]
Load 0A	**5.9**	**6**
Load 50A	**28**	**25**

Fig. 6. Experimental result and graph of the position error

IV. Experimental Verifications and Design of the Motor for Sensorless Control

A. Experimental verifications

The following shows the experimental verifications of the models. Fig. 4 is the Photographs of the test set. From the waveform of the phase inductance according to the load state

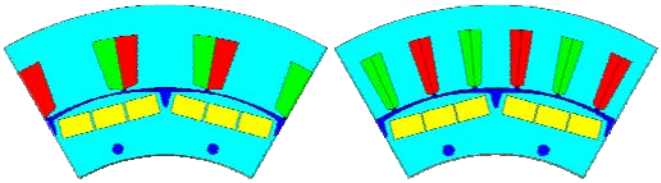

(a) Concentrated winding (b) distributed winding

Fig. 7. Design models with winding combination

TABLE II
DESIGN PROPERTIES AND PARAMETER FOR SENSORLESS CONTROL

	Concentrated model	Distributed model
Pole/Slot	12/18	12/36
Rated torque [Nm]	50	50
Remanent flux density [T]	1.126	1.237
THD of inductance [%] (@ rated load 50A)	45.2	9.1
Magnetic loading [kA/m]	1.0	1.3
Electric loading [mWb]	107.2	69.0

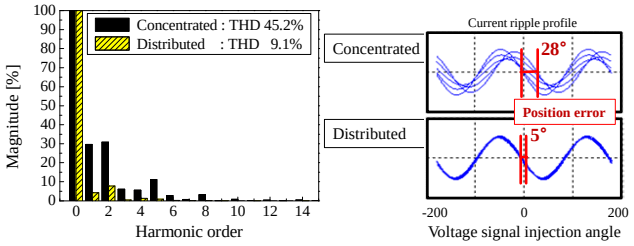

Fig. 8. Distortion of the phase inductance and the estimated current ripple

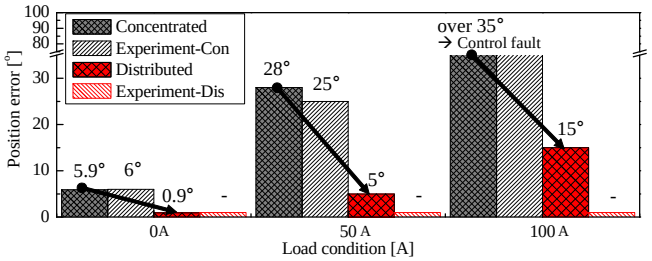

Fig. 9. Comparison of the rotor position error with winding combination

in Fig. 1, the current ripple waveform (inverse values of the inductances) changed by the rotor position under no-load and load conditions is shown in Fig. 5. As many *n-th* order harmonics are contained in the phase inductance matrix, the estimation error is increased. Fig. 6 compares the estimated position error under no-load and load consitions with the experimental results. The error is displayed in the form of 6th-order harmonics.

B. Design results for sensorless control in IPMSM

Fig. 7 shows an electric motor for comparing the sensorless control properties. These are the models that have been optimally designed moderately with concentrated winding of 12-poles 18-slots and distributed winding of 12-poles 36-slots [7-9]. From the Section 3, the design conditions for the rotor position computation is shown in Table 2. From the change of the winding and the increase in magnetic loading, the cause of the two conditions is clear. In Fig. 8, the distorted waveforms through the phase inductance of the motor were compared between, and the current ripple that have been converted from the waveform of the phase inductance is shown under load 50A. In the figure, it is shown that both the magnetic loading and the winding type can cause a reduction of the position estimating errors. Fig. 9 shows the result of estimating the position of the rotor as a winding type in the sensorless control method. The motor designed the distributed winding can be seen that the position errors of the rotor is smaller. Further, it was verified that it is possible to determine the design concept of the electric motor for sensorless control.

V. CONCLUSION

In this paper, the cause of the estimating position error was examined to clarify the sensorless control method. The design of an electric motor for reducing the position error is described. The THD of the phase inductance is one of the key factors for designing motors for sensorless control. In order to reduce the distortion of the phase inductance profile, an electric-/magnetic-loading and the winding combination is considered. The high level of the magnetic loading and the distributed winding are optimized making the design concept of a motor with stable sensorless controlled capability possible.

ACKNOWLEDGMENT

This research was supported by the MKE (The Ministry of Knowledge Economy), Korea, under the CITRC (Convergence Information Technology Research Center) support program (NIPA-2013-H0401-13-1008) supervised by the NIPA (National IT Industry Promotion Agency).

REFERENCES

[1] S. M. Kim, J. I. Ha and S. K. Sul, “PWM switching frequency signal injection sensorless method in IPMSM”, *IEEE Trans. on Ind. Appl.*, vol. 48, No. 5, pp. 1576-1587, 2012.

[2] Y. Kano, T. Kosaka, N. Matsui and M. Fujitsuna, “Sensorless-oriented design of concentrated winding IPM motors for HEV drive application”, *in conf. Rec. IEEE ICEM*, pp. 2709-2715, 2012.

[3] Y. Li, Z. Q. Zhu, D. Howe and C. M. Bingham, “Modeling of cross-coupling magnetic saturation in signal-injection-based sensorless control of permanent-magnet brushless AC motors”, *IEEE Trans. Magn.*, vol. 43, No. 6, pp. 2552-2554, June, 2007.

[4] Z. Q. Zhu, Y. Li, D. Howe and C. M. Bingham, “Compensation for rotor position estimation error due to cross-coupling magnetic saturation in signal injection based sensorless control of PM brushless AC motor”, *in conf. Rec. IEEE IEMDC*, pp. 208-213, 2007.

[5] N. Bianchi and S. Bolognani, “Influence of rotor geometry of an IPM motor on sensorless control feasibility”, *IEEE Trans. on Ind. Appl.*, vol. 43, No. 1, pp. 87-96, Jan.-Fab., 2007.

[6] L. Chong and M. F. Rahman, “Comparison of d- and q-axis Inductances in an IPM Machine with Integral-slot Distributed and Fractional-slot Concentrated Windings”, *Electrical Machines, ICEM 2008*. pp. 1-5, 2008.

[7] Y. Kano, T. Kosaka, N. Matsui and T. Nakanishi, “Design and experimental verification of a sensorless-oriented concentrated-winding IPMSM,” *in conf. Rec. IEEE ICEM*, pp. 1-6, Sept., 2010.

[8] Sung-Il Kim, Jung-Pyo Hong, Young-Kyoun Kim, Hyuk Nam and Han-Ik Cho, “Optimal design of slotless-type PMLSM considering multiple responses by response surface methodology,” *IEEE Trans. Magn.*, vol. 42, No. 4, pp. 1219-1222, April 2006.

[9] B. H. Lee, J. P. Hong, J. H. Lee and S. M. Jang, “Optimum design criteria for maximum torque and efficiency of a line-start permanent-magnet using response surface methodology and finite element method,” *IEEE Trans. Magn.*, vol. 48, No. 2, pp. 863-866, Feb. 2012